Conformal atomic layer deposition of RuOx on highly porous current collectors for micro-supercapacitor applications

Sakeb Hasan Choudhury, Guillaume Vignaud, Pascal Dubreuil, Birhanu Desalegn Assresahegn, Daniel Guay, David Pech

Conformal Atomic Layer Deposition of RuO_x on highly porous current collectors for micro-supercapacitor applications

Sakeb Hasan Choudhury[1], Guillaume Vignaud[2], Pascal Dubreuil[1], Birhanu Desalegn Assresahegn[3], Daniel Guay[3] and David Pech[1]

[1] LAAS-CNRS, Université de Toulouse, CNRS, 7 avenue du colonel Roche, Toulouse 31400, France.
[2] Institut de Recherche Dupuy de Lôme (IRDL), UMR CNRS 6027, Université Bretagne Sud, Rue St Maudé, 56100 Lorient, France.
[3] INRS-Énergie, Matériaux et Télécommunications, 1650 Boulevard Lionel Boulet, Varennes, C.P. 1020, Québec J3X 1P7, Canada.

E-mail: dpech@laas.fr

Abstract

3D porous electrodes have been considered as a new paradigm shift for increasing the energy storage of pseudocapacitive micro-supercapacitors for on-chip electronics. However, the conformal deposition of active materials is still challenging when highly porous structures are involved. In this work, we have investigated the atomic layer deposition (ALD) of ruthenium dioxide RuO_2 on porous Au and Pt architectures prepared by hydrogen bubble templated electrodeposition, with area enlargement factors (AEF) ranging from 400 to 10000 cm^2/cm^2. Using proper ALD conditions, a uniform RuO_2 coverage has been successfully obtained on porous Au, with a specific electrode capacitance of 8.1 mF cm^{-2} and a specific power of 160 mW cm^{-2} for a minute amount of active material. This study also shows the importance of the chemical composition and reactivity of the porous substrate for achieving conformal deposition of a ruthenium oxide layer.

Keywords: RuO_x, ALD, porous substrate, DHBT, micro-supercapacitor,

1. Introduction

The availability of autonomous microelectronic devices is set to revolutionize the IoT (Internet of Things) based industry. Indeed, the production of self-powered microelectronic devices that incorporate energy conversion and energy storage units is regarded as a gamechanger for future technologies considering its compatibility with multiple application fields such as manufacturing, industrial automation, healthcare, environmental monitoring, traffic management [1]. Modern stand-alone wearable electronics and wireless sensor networks demand high-density onboard power/energy supply. In this respect, micro-supercapacitors are viewed as prime candidates as they are demonstrating high power density with extraordinary cycling stability. Up to now, micro-supercapacitors needed to be coupled with micro-batteries because of their inherent low energy densities. However, with the emergence of micro-supercapacitors based on 3D architectures [2], this limitation no longer exits and they are considered as stand-alone components thanks to much higher energy density (while keeping high power density and cycling stability). In recent years, 3D micro-supercapacitors have emerged as efficient energy storage devices to bridge the gap of practical-requirement of on-board micro-energy devices.

Several approaches were followed to make 3D micro-supercapacitor electrodes. Top-down microfabrication

methods based on micromachining processes have been investigated to realize 3D microstructures comprised of deep trenches, pillars and walls [3], but their adequateness to large-scale production is questionable in terms of time, process complexity, and economic perspectives. At the other hand of the spectrum, bottom-up approaches have also been used to prepare 3D microstructures, based on the spontaneous self-organization of small entities to form structures with long-range order. Among various bottom-up techniques, the dynamic hydrogen bubble template (DHBT) method is very interesting and was investigated for different applications such as micro-batteries [4], catalysis and sensing, among others [5].

DHBT is a versatile electrodeposition method to prepare deposits with controlled nano- and micro-porosity that can then be used as porous current collectors. They are characterized by good mechanical stability and excellent electronic conductivity while allowing easy electrolyte percolation through the open structure. Aside from the advantage of the 3D structure, the porosity and thickness of the DHBT deposits can be controlled precisely through the deposition parameters, typically the current density and the deposition time. Furthermore, the porosity of DHBT deposits can be further increased by de-alloying one of the metallic components from the initial bimetallic deposit [6]. Adopting this particular methodology, we were able to prepare highly porous metallic current collectors with incredibly large area enlargement factors (AEF), up to 10000 cm^2 per cm^2 [7]. This porous support was then entirely embedded by a thick film of pseudocapacitive hydrated ruthenium dioxide RuO_2 using an electrodeposition technique. Although extremely high capacitances were achieved, the active material blocked a significant fraction of the surface of the porous current collector. Accordingly, a substantial portion of the electrodeposited ruthenium dioxide was unable to contribute to the energy storage mechanism. Moreover, these high capacitances were accompanied by a lower charge/discharge rates compared with conventional supercapacitors [8].

Therefore, in order to enhance the effective surface area of RuO_2, the main issue to address here is the conformal deposition of a very thin film of RuO_2 on these high aspect ratio structures. In this work, we propose an alternative method for the deposition of hydrous RuO_x into DHBT structures using atomic layer deposition (ALD) to ensure high effective surface area and enhanced active mass utilization. Moreover, the efficient utilization of an ultra-thin layer of RuO_x makes the manufacture of 3D micro-supercapacitors economically feasible. We strategically pre-selected two different 3D metallic electrodes, one based on Au and one based on Pt, to achieve an overview of how the ALD can accommodate moderate (Au) and high (Pt) porosity scaffolds.

2. Experimental section

2.1 Electrochemical deposition of Au and Pt current collector

A Ti(50 nm)/Au(300 nm) thin film was deposited by evaporation on an oxidized silicon substrate first. DHBT deposition of Au was electrochemically deposited on top of the evaporated Au film. For DHBT deposition of Au, the electrolytic bath solution was prepared by dissolving 2 mM $H_3AuCl_4.3H_2O$ in an aqueous solution of 3 M H_2SO_4. Au DHBT was electrodeposited using a constant current protocol (5 A cm^{-2}) in a 3-electrode configuration for different durations. The thickness of Au DHBT was controlled by the duration of electrodeposition.

Similarly, a Ti(50 nm)/Pt(200 nm) thin film was deposited by evaporation on an oxidized silicon substrate for the DHBT deposition of Pt. DHBT deposition of Pt was electrochemically deposited on top of the evaporated Pt film. In that case, Pt/Cu DHBT alloy was first electrodeposited at room temperature using an aqueous bath containing 0.03 M H_2PtCl_6 and 0.015 M $CuSO_4.5H_2O$ salts diluted in 1 M H_2SO_4, using a constant current protocol (6.5 A cm^{-2}) in a 3-electrode configuration for different durations. Afterwards, Cu was electrochemically de-alloyed through cyclic voltammetry (CV) in 0.5 M H_2SO_4 between -0.38 and + 1.2 *vs.* SCE for 50 cycles at 10 mV s^{-1}. The sample obtained after Cu de-alloying was termed as Pt(Cu) DHBT.

2.2 Atomic layer deposition of RuO_x

ALD was performed in a SI ALD LL system from Sentech. We used bis-(ethylcyclopentadienyl) ruthenium $Ru(EtCp)_2$ and O_2 as precursors for the deposition of RuO_x. $Ru(EtCp)_2$ and O_2 were pulsed for 1 and 15 s, respectively. In order to remove the unreacted precursor and gas phase reaction products, the system was purged with Ar during 40 s between each successive pulse.

Different substrates were used. Flat Au and Pt substrates were used for ellipsometry measurements. Au and Pt(Cu) DHBT substrates were used for electrochemical characterizations. These substrates were prepared as described above. The temperature for ALD deposition was changed from 200 to 350°C. However, the film deposition below 250°C was almost untraceable by ellipsometer. So, in the following, RuO_x ALD deposition on both Au and Pt(Cu) DHBT substrates was performed at 300 and 350°C.

2.3 Characterizations

Electrochemical characterizations of the samples were performed using an EC-Lab BioLogic VMP3 potentiostat in a 3-electrode configuration in 0.5 M H_2SO_4 electrolyte at room temperature. A Pt mesh was used as the counter electrode and a saturated Ag/AgCl was used as the reference

electrode. The surface morphology of the DHBT samples was examined by scanning electron microscopy (SEM) performed on a Hitachi S-4800 field emission electron microscope operating at 5 kV. X-ray photoelectron spectroscopy (XPS) analysis was performed with a Thermo Scientific spectrometer operating with a monochromatic Al Kα X-ray source (1486.6 eV). For measuring the thickness of the RuO_x ALD deposits, a Jobin Yvon−Uvisel ellipsometer instrument was used. It consists of a Xe source, with wavelength ranging from long-range infrared to ultraviolet (250–1700 nm), a polarizer, an analyzer, and a monochromator handling the dispersion and the selection of the wavelength to a photomultiplier.

2.4 Area Enlargement Factor (AEF) calculation

The "Area Enlargement Factor" (AEF) was used to evaluate the increased surface area of the DHBT structures using the following formulae:

$$\text{AEF} = \text{Electrochemical Active Surface Area (EASA)} / \text{Geometrical Area}$$

The EASA of gold electrodes was calculated from CVs using a specific charge density of 390 μC cm^{-2} for the gold oxide reduction process [9]. In the case of Pt(Cu) DHBT, the electrochemical surface area of porous Pt electrodes was calculated by integrating the charge of the hydrogen desorption peaks of CVs taken in 0.5 M H_2SO_4, using a specific charge density for the desorption of hydrogen on Pt of 210 μC cm^{-2} [7].

3. Results and discussions

3.1 ALD growth characteristics of RuO_x on flat substrates

To understand the ALD growth mechanism of RuO_x using $Ru(EtCp)_2$ precursor and O_2, we started by investigating the growth of RuO_x layer on a Si wafer with native oxide, a flat 300 nm-thick Au and 200 nm-thick Pt substrates. These flat substrates were subjected to RuO_x deposition by ALD with different number of cycles and different deposition temperatures. The ALD deposition temperature was varied from 200 to 350°C. Figure 1(a) shows the evolution of the RuO_x film thickness, obtained from ellipsometry measurements, with the number of ALD cycles performed at 350°C using different flat substrates. The growth of RuO_x on flat Au substrate shows a linear correlation with the number of ALD cycles, with a growth rate of 0.027 Å per cycle. A similar trend could not be confirmed for Pt or Si substrate.

It was previously reported that ALD RuO_x deposition using $Ru(EtCp)_2$ and O_2 suffers from a nucleation delay on Si substrate, and more than 500 ALD cycles were needed before obtaining a continuous film [10]. This non-uniform ALD RuO_x growth is consistent with our results on Si and Pt substrates from scanning electron microscopy (SEM) observations (figure S1). From our ellipsometry data, the measured film thickness confirms a similar outcome that RuO_x island formation takes place below 500 ALD cycles on Si and Pt. This can be interpreted as the measured constant film thickness observed below 500 ALD cycles. However, the progress of RuO_x deposition seems different in case of flat Au as the film thickness shows a linear correlation with number of ALD cycles up to 1000 cycles with no nucleation delay. Aside from this, a smooth and flat morphology was inspected from the SEM images regardless of ALD deposition temperature (figure S1). These results indicate a homogenous ALD RuO_x film on top of flat Au and a steady ALD RuO_x growth process.

Figure 1(b) shows the cyclic voltammograms, recorded at different scan rates, of a flat Au substrate covered with RuO_x deposited after 500 ALD cycles. All CVs exhibit the typical pseudocapacitive profile expected from hydrous RuO_x film with negligible resistive contributions. Moreover, the specific capacitance increases linearly with increasing number of ALD cycles (figure S2).

To study the optimal of ALD deposition temperature, different number of ALD cycles were deposited on flat Au and flat Pt at temperatures varying from 200 to 350°C (figure 1(c)). At the lowest deposition temperature (200°C), there is almost no effect of the number of deposition cycles on the specific capacitance, suggesting no RuO_x is deposited to any significant extent at this deposition temperature. At that temperature, the specific capacitance was *ca.* 0.11 mF cm^{-2}, which corresponds to the capacitance of flat Au film with AEF of *ca.* 2-3. Increasing the deposition temperature starts to reveal the impact of the pseudocapacitive performance of the ALD grown RuO_x with a favourable temperature window for ALD deposition beginning from 300°C and onwards.

3.2 ALD on porous Au current collectors

Replicating the conformal deposition of RuO_x achieved by ALD on planar Au substrates to the intricate Au DHBT structure appears to be challenging due to the extremely high porosity of the substrate. During DHBT deposition, the DHBT film sprouts with complex scaffold-like structures, with pore diameter ranging from 5-100 μm depending on the deposition time and material, and with interconnected pore walls due to random nucleation and dendritic growth (figure S3). The surface morphology of DHBT structure also varies for different metallic systems. In figure 2(a) and 2(b), a comparison of the surface morphology of the Au DHBT substrate before and after RuO_x deposition (500 cycles at 350°C) is presented. After the conformal deposition of RuO_x, all the structural attributes of the Au DHBT substrate appear to be unaffected. It also verifies that these porous 3D

structures of Au DHBT maintain its robust architecture, chemical stability, mechanical strength and furthermore exhibit a strong adherence to the substrate. The XPS spectra of the Ru 3d, Ru 3p and O 1s core level are shown are in figure 2(c) and S4. No trace of metallic Ru is observed, with peaks corresponding to ruthenium dioxide, as previously reported [11]. The cross-section SEM image of Au DHBT substrate after RuO_x deposition can be found in figure 2(d). The structure of electrodeposited Au DHBT can be observed very clearly. In the image, the area of Au DHBT channels with ALD RuO_x that are exposed to the electrolyte is marked with blue rectangles. The results of the EDS mapping on the surface of the Au DHBT with 500 cycles at 350°C is shown in figure 2(e) and 2(f). From the EDS mapping, it can be found that RuO_x is conformally deposited on the surface of Au DHBT. Therefore, ALD allows the direct deposition of the pseudocapacitive RuO_x active material without requiring any additional oxidation step.

To electrochemically characterize conformally grown ALD RuO_x deposits, different thicknesses and porosities of the Au DHBT substrates were considered. The thickness of the Au DHBT substrate was controlled by varying the duration of the DHBT electrochemical deposition process. The CVs of the bare Au DHBT substrates are displayed in figure 3(a), where the DHBT electrodeposition time is varied from 5 to 20 min. As a result of higher thickness of Au DHBT, the area under the Au oxide reduction peak at 0.88 V *vs.* Ag/AgCl is increasing with the deposition time. The corresponding mass gain and thickness for different DHBT deposition time are plotted in figure 3(b). The surface area enhancement (AEF) factor ranges from 195 to 398 cm^2/cm^2 after 5 to 20 min of electrodeposition (figure 3(c)).

CV measurements were performed on Au DHBT samples of different thickness plus 1000 cycles of conformal ALD RuO_x (figure 3 (d)). The current profiles from cyclic voltammetry of all samples portray an almost symmetrical and rectangular shape as expective for pseudocapacitive materials. A specific capacitance of 8.1 mF cm^{-2} is obtained on the 20 min DHBT current collector – which is 22 times larger than that obtained on the bare Au DHBT substrate (372 µF cm^{-2}) – with a specific energy density reaching 2.6 mJ cm^{-2} (i.e. 0.7 µWh cm^{-2}). The sweep-rate dependence of the recorded current is shown in figure 3(e). A linear dependency between log(current *i*) *vs.* log (scan rate *s*) is observed for all samples. The slope of the log(*i*) *vs.* log(*s*) is 1, indicating that the overall response tends to be capacitive [12] with an easy and efficient access of the electrolyte to the porous architecture, facilitating fast reversible redox reactions. Figure 3(f) shows the Nyquist plot for the same samples. No leakage current is observed, with a near vertical line in the low-frequency region representative of a capacitive behaviour. Additionally, the impedance value decreases with increasing AEF of the Au DHBT, in agreement with a higher capacitance of the electrodes. A very low equivalent series resistance (ESR), of the order of 0.8-1 Ω cm^2, is found for all the samples, with an estimated a high specific power density of 160 mW cm^{-2}. In order to check the stability of the combined ALD RuO_x/Au DHBT structure SEM imaging was done after electrochemical characterization. The images are shown in figure S5 which confirms that the overall structure and morphology of Au DHBT with ALD RuO_x is consistent after electrochemical characterization.

Therefore, we showed that ruthenium dioxide can be deposited at the surface of Au DHBT electrode with an AEF of 398 cm^2/cm^2 using a one-step thermally-assisted ALD process. In order to investigate the limit of ALD, we study in the next section how the same process can be used to deposit RuO_x on a porous substrate with an AEF of 10000 cm^2/cm^2.

3.3 ALD on porous Pt(Cu) current collectors

Highly porous Pt current collectors having tremendous AEF were prepared by combining PtCu alloy DHBT electrodeposition followed by a partial dissolution of Cu via an electrochemical Cu de-alloying step.

Figures 4(a) shows the CVs of Pt(Cu) DHBT after different DHBT electrodeposition time. The calculated AEF of the corresponding Pt(Cu) DHBT substrates, calculated from the area under the hydrogen desorption peaks, are indicated. The maximum AEF reaches a prodigious value of ~ 10000 cm^{-2}/cm^{-2} for 10 min Pt(Cu) DHBT deposition. This extremely high porosity is not achievable through the DHBT deposition of Pt alone. It unveils the advantage of performing co-deposition of Pt and Cu and the subsequent leaching out of Cu to add nanoscale porosity. Moreover, this particular methodology overcomes the lack of adequate adhesion of Pt DHBT on the substrate [7]. SEM images captured from the surface morphology of Pt(Cu) DHBT after Cu de-alloying are shown in figure 4(b). The cauliflower-like structures of Pt(Cu) DHBT are clearly discernible from high-resolution images. During the deposition, Pt forms a three-dimensional solid structure compared to a sea weed/leaf-like frames of Au DHBT.

Figure 4(c) shows the Ru 3d core level spectra (XPS measurements) of a Pt(Cu) DHBT sample with 500 cycles of ALD. The binding energy of Ru $3d_{5/2}$ peak appears to be at ~280.8 eV. Using the reference from previous work [13], we found that the ALD deposited RuO_x represents a convoluted spectrum of crystalline RuO_2 and hydrous RuO_2.

For electrochemical characterizations, we deposited ALD RuO_x on a 5 min de-alloyed Pt(Cu) DHBT substrate with post Cu de-alloying. Figure 4(d) shows the CVs performed in 0.5 M H_2SO_4 at different scan rates, from 10 mV s^{-1} to 1 V s^{-1}, for 250 cycles of ALD RuO_x. All CVs possess similar current profiles distinct from the ones expected for hydrous ruthenium oxide. Indeed, very distinct redox peaks are

observed at *ca.* 0.5 V *vs.* Ag/AgCl that are attributed to the oxidation/reduction of the remaining Cu (~26 at.% after de-alloying) from the DHBT structure [7]. We believe that O_2 used in the thermal ALD process oxidizes the Cu atoms remaining in the substrate after de-alloying, forming Cu_2O compound. Therefore, the oxidation/reduction peak may be attributed to the Cu_2O/CuO redox couple [14,15]. Figure 4(e) shows the CVs performed at 250 mV s^{-1} in 0.5 M H_2SO_4 with increasing number of ALD cycles at 350°C. The CV of Pt(Cu) DHBT substrate performed within the same potential range (0.1 – 0.9 V *vs.* Ag/AgCl) is given as a reference. The redox peak increases with increasing number of ALD cycles, and consequently the period where the substrate is heated (350°C) in presence of oxygen. It is inferred that the heat treatment during the ALD process and the presence of O_2 result in a higher diffusion of Cu from the bulk and the formation of more Cu_2O.

Figure 4(f) shows the Nyquist plots with increasing number of ALD cycles, from 250 to 1000 cycles. All plots show an almost capacitive-like behaviour with semicircles at high frequencies, related to the distributed resistance/capacitance of the porous electrode [16, 17]. Increasing the number of ALD cycles enhances the capacitance of the electrode, suggesting that some RuO_x is also deposited inside the highly porous Pt(Cu) DHBT scaffold, which is consistent with the XPS results (figure 4(c)). However, to get an efficient ALD of RuO_x, the substrate should not contain elements more oxidizable than Ru.

4. Conclusions

Through our work, we have established that the whole preparation methodology, starting from DHBT and ALD RuO_x, is perfectly scalable and tuneable to the practical requirement of micro-supercapactior application. Our scientific work highlights that an ultra-thin ALD RuO_x can satisfy the economical aspect of 3D micro-supercapactior fabrication compared to other deposition methods. Considering the fundamental ALD process, our research confirmed that ALD growth of RuO_x is attainable on a flat Au sample and deposition conditions can be further transferred to conformally coat Au DHBT structure with moderate porosity. On the contrary, a continuous uniform RuO_x layer could not be accomplished on flat Pt by the same ALD process for the lack of homogenous nucleation. The mixed redox peaks and the pseudocapacitive response observed for RuO_x ALD deposited on a Pt(Cu) DHBT substrate indicate the need to find another alloying element M for the Pt(M) DHBT substrate. Therefore, the choice of a suitable substrate is a prerequisite for the conformal deposition of pseudocapacitive RuO_x active material by the thermally assisted ALD process.

Acknowledgements

The authors acknowledge the support from the European Research Council (ERC) under the European Union's Horizon 2020 research and innovation programme (ERC-2017-CoG, grant agreement n°771793 3D-CAP). This work was supported by LAAS-CNRS technology platform, a member of Renatech network.

References

[1] Lethien C, Le Bideau J and Brousse T 2019 *Energy Environ. Sci.* **12** 96-115

[2] Kyerematen N A, Brousse T and Pech D 2017 *Nat. Nanotechnol.* **12** 7-15

[3] Eustache E, Douard C, Demortière A, De Andrade V, Brachet M, Le Bideau J, Brousse T and Lethien C 2017 *Adv. Mater. Technol.* **2** 1700126

[4] Patnaik S G and Pech D 2021 *Small* **17** 2101615

[5] Plowman B J, Jones L A and Bhargava S K 2015 *Chem. Commun.* **51** 4331

[6] Ferris A, Bourrier D, Garbarino S, Guay D and Pech D 2019 *Small* **15** 1901224

[7] Karroubi L B, Patnaik S G, Assresahegn B D, Bounor B, Tran C C H, Choudhury S H, Bourrier D, Guay D and Pech D 2022 *Energy Storage Mater.* **47** 134-40

[8] Ferris A, Garbarino S, Guay D and Pech D 2015 *Adv. Mater.* **27** 6625-9

[9] Trassatti S and Petrii A 1991 *Pure & Appl. Chem.* **63** 711-34

[10] Salau¨n A, Newcomb S B, Povey I M, Salau¨n M, Keeney L, O'Mahony A and Pemble M E 2011 *Chem. Vap. Deposition* **17** 114–122

[11] Rochefort D, Dabo P, Guay D and Sherwood P M A 2003 *Electrochim. Acta* **48** 4245-52

[12] Ferris A, Reig B, Eddarir A, Pierson J-F, Garbarino S, Guay D and Pech D 2017 *ACS Energy Lett.* **2** 1734-9

[13] Patnaik S G, Seenath J S, Bourrier D, Prabhudev S, Guay D and Pech D 2021 *ACS Energy Lett.* **6** 131-9

[14] Grishina E P, Udalova A M and Rumyantsev E M 2002 *Russ. J. Electrochem.* **38** 1041-4

[15] Sachin D G and Sarkar A 2016 *J. Electrochem. Soc.* **163** H252-9

[16] Alison A and Andreas H A 2019 *J. Power Sources* **426** 93-6

[17] Laschuk N O, Easton E B and Zenkina O V 2021 *RSC Adv.* **11** 27925

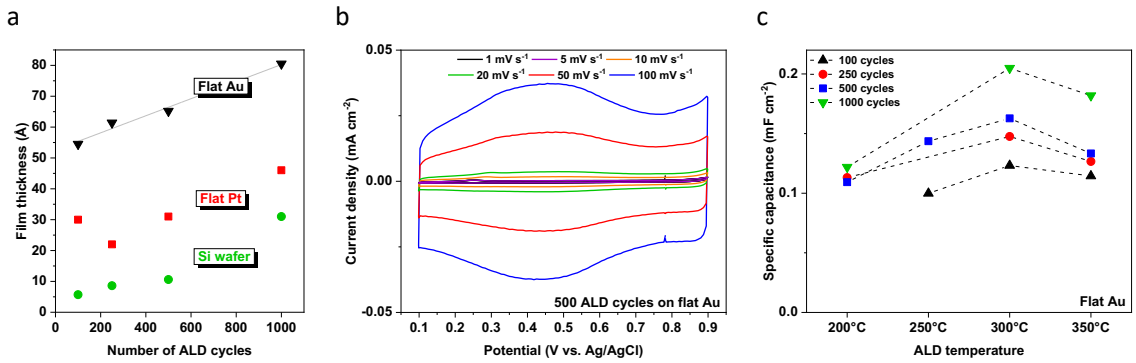

Figure 1. ALD on flat substrates. (a) Evolution of the film thickness *vs.* the number of ALD cycles at 350°C. (b) Cyclic voltammograms in 0.5 M de-aerated H_2SO_4 of 500 ALD cycles deposited on flat Au. (c) Evolution of the specific capacitance *vs.* ALD temperature on flat Au.

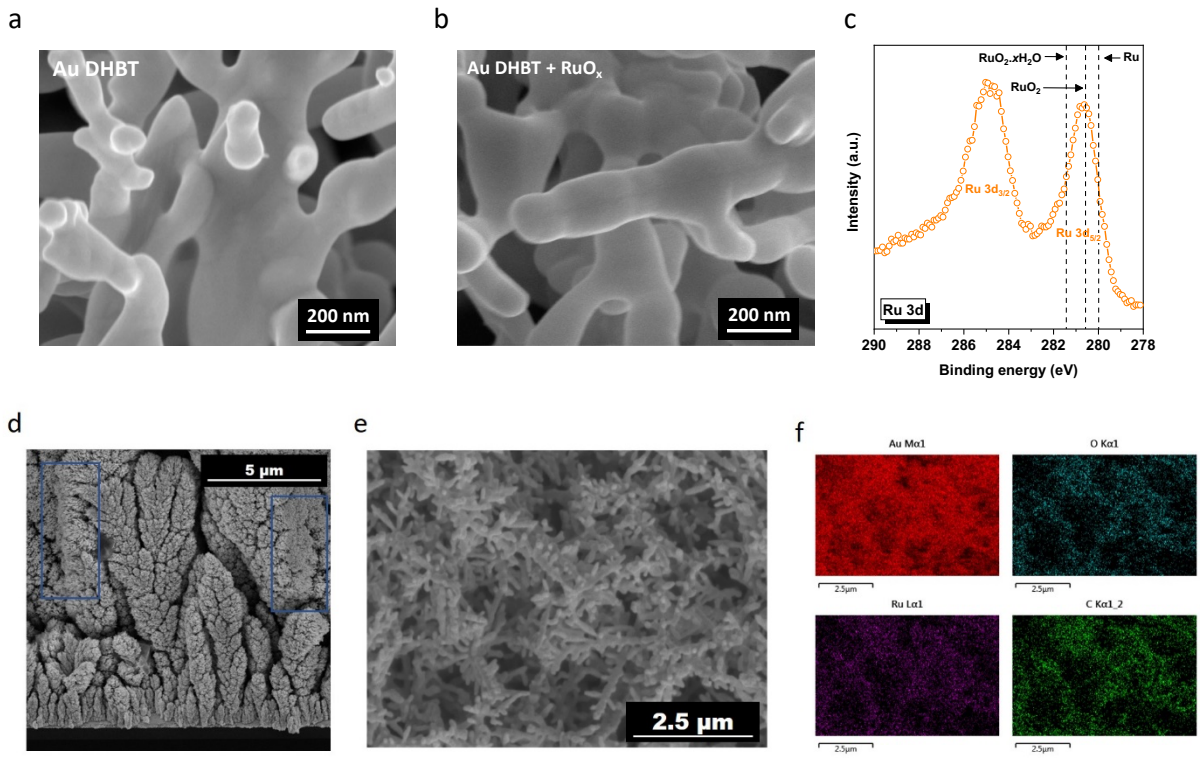

Figure 2. ALD on Au DHBT. SEM image before (a) and after (b) 500 ALD cycles at 350°C. (c) Ru 3d core-level XPS spectrum after 500 ALD cycles showing the deposition of oxidized ruthenium. Cross-section SEM image of Au DHBT with 500 ALD cycles at 350°C (d). The areas identified with the blue rectangles are the exposed area of Au DHBT channels with ALD RuOx. The EDS mapping was performed on the SEM image shown in figure (e) and the corresponding elemental mapping can be found in figure (f).

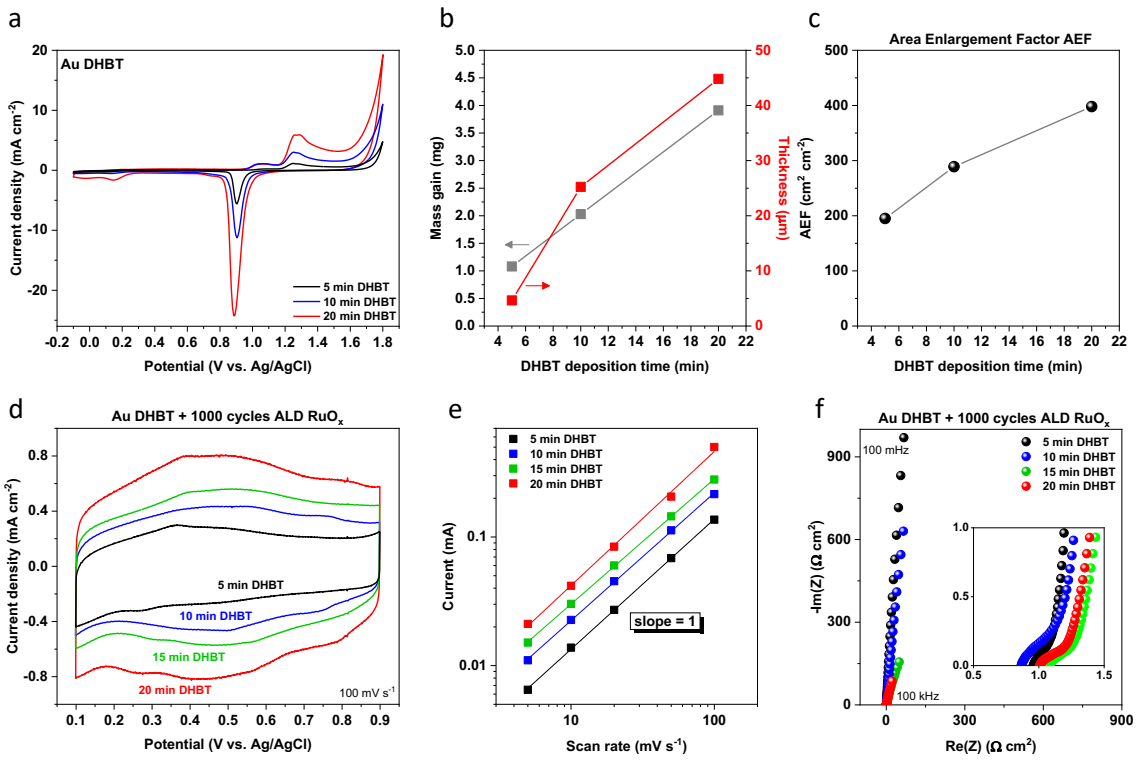

Figure 3. ALD on Au DHBT. (a) CVs of the porous DHBT Au after different electrodeposition time in de-aerated 0.5 M H_2SO_4. (b) Mass gain and thickness of Au DHBT substrate, (c) AEF increment with increasing DHBT deposition time. (d) CVs after 1000 ALD cycles on different Au DHBT substrates with different thicknesses. (e) Corresponding sweep-rate *s* dependence of the current *i*: the slope of the plot log(*i*) vs. log (*s*) is 1. (f) Nyquist plot of the different RuO_x / Au DHBT electrodes (inset: high-frequency region).

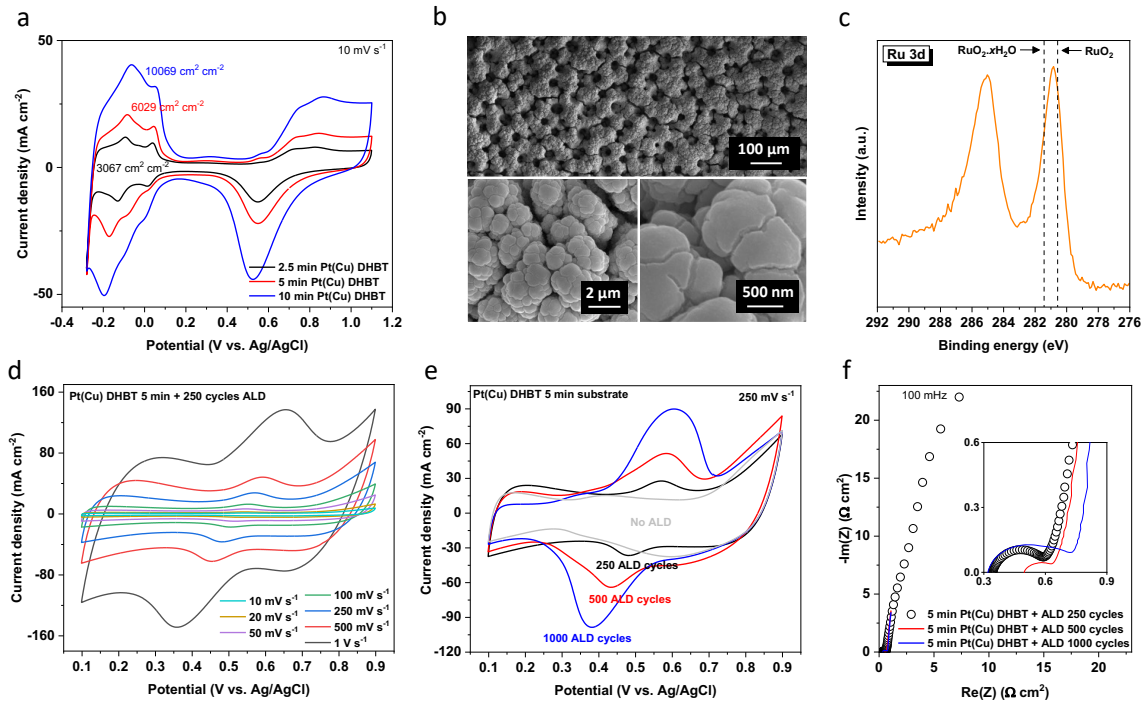

Figure 4. ALD on Pt(Cu) DHBT. (a) CVs of the porous Pt(Cu) DHBT after different electrodeposition time in de-aerated 0.5 M H_2SO_4 after Cu de-alloying. (b) SEM images of Pt(Cu) DHBT at different magnifications. (c) Ru 3d core-level XPS spectrum after ALD. (d) CVs after 250 ALD cycles at different scan rates in de-aerated 0.5 M H_2SO_4. (e) CVs at 250 mV s^{-1} of Pt(Cu) DHBT with different number of ALD cycles and (f) evolution of the Nyquist plot (inset: high-frequency region) with increasing number of ALD cycles performed at 350°C.